



## CeO<sub>2</sub> nanoparticles supported on CuFe<sub>2</sub>O<sub>4</sub> nanofibers as novel adsorbent for removal of Pb(II), Ni(II), and V(V) ions from petrochemical wastewater

Fatemeh Talebzadeh<sup>a</sup>, Raziye Zandipak<sup>a</sup>, Soheil Sobhanardakani<sup>b,\*</sup>

<sup>a</sup>Young Researchers & Elite Club, Hamedan Branch, Islamic Azad University, Hamedan, Iran, emails: [f.talebzadeh@iauh.ac.ir](mailto:f.talebzadeh@iauh.ac.ir) (F. Talebzadeh), [raziyeh.zandi@yahoo.com](mailto:raziyeh.zandi@yahoo.com) (R. Zandipak)

<sup>b</sup>Department of the Environment, College of Basic Sciences, Hamedan Branch, Islamic Azad University, Hamedan, Iran, Tel./Fax: +98 8134494143; email: [s\\_sobhan@iauh.ac.ir](mailto:s_sobhan@iauh.ac.ir)

Received 10 February 2016; Accepted 26 April 2016

### ABSTRACT

In the present work, the CeO<sub>2</sub>/CuFe<sub>2</sub>O<sub>4</sub> nanofibers with the structure of CuFe<sub>2</sub>O<sub>4</sub> as the core and CeO<sub>2</sub> nanoparticles as the outer layer were prepared. This novel nanostructure was characterized by X-ray diffraction analysis, Fourier transform infrared spectroscopy, and scanning electron microscopy (SEM). The sizes of CeO<sub>2</sub>/CuFe<sub>2</sub>O<sub>4</sub> nanofibers determined from the SEM images were 100 nm. The obtained nanocomposite was used to investigate adsorption of Pb(II), Ni(II), and V(V) ions from aqueous solutions. Contact time, pH, initial metal concentration, and temperature were optimized to improve the removal efficiency. The adsorption equilibrium and kinetic data were modeled with classical and recently developed models. Maximum adsorption capacity of Pb(II), Ni(II), and V(V) on CeO<sub>2</sub>/CuFe<sub>2</sub>O<sub>4</sub> nanofibers were 972.4, 686.1, and 798.6 mg g<sup>-1</sup>, respectively. The results showed that the synthesized nanocomposite could be considered as an efficient adsorbent in the field of wastewater treatment.

*Keywords:* CeO<sub>2</sub>/CuFe<sub>2</sub>O<sub>4</sub> nanofibers; Adsorption; Non-linear; Metal ions

### 1. Introduction

Contamination of water systems with heavy metals received an increasing attention in the last decades. Heavy metals are generally considered to be one of the most important inorganic pollutants due to their toxicity toward living organisms [1]. Of all the heavy metals, lead (Pb), nickel (Ni), and vanadium (V) are carcinogenic and non-biodegradable substance, and it is commonly detected in textile dyeing, petroleum refining, tanneries, steel, ceramic, glass, galvanization, smelting, and mineral processing wastewater [2,3].

The presence of metal ions in drinking water can cause adverse effects in humans such as anemia, encephalopathy, nausea, diarrhea, headache, cancer of lungs, dermatitis, hepatitis, nephritic syndrome the kidneys, and the dysfunction of reproductive and central nervous system. According to the World Health Organization (WHO), the permissible limit of Pb, Ni, and V for drinking water is 0.01, 0.1, and 0.015 mg L<sup>-1</sup>, respectively [4–6]. Up to now, researchers have tried to remove heavy metal ions by various methods, including membrane separation, precipitation, ion-exchange, electrochemical reduction, reverse osmosis, and adsorption [7,8]. Among them, adsorption is an easy and economic process due to its high

\*Corresponding author.

selectivity, simplicity of design, and separation of various pollutants [9].

Nanomagnetic materials are considered potential adsorbents for removal of pollutants due to their high surface area and the unique advantage of easy separation under external magnetic fields. Several reports have been published on the using of various types of nanomagnetic materials for removal, separation, and determination of dyes and metal ions [10].

Nanocrystalline ferrites with the general formula  $MFe_2O_4$  ( $M = Mn, Co, Ni, Cu, \text{ or } Zn$ ) are very important magnetic materials because of their interesting magnetic and electrical properties with chemical and thermal stabilities. Among the ferrites, copper ferrites ( $CuFe_2O_4$ ) have attracted much fundamental and applied research attention owing to its wide applications in sensors, electronics, catalysts, and removal of heavy metals.  $CuFe_2O_4$  with an inverse spinel structure shows ferrimagnetism that originates from magnetic moment of anti-parallel spins between  $Fe^{3+}$  ions at tetrahedral sites and  $Cu^{2+}$  ions at octahedral sites [11,12].

So far, most reported nanostructures  $CuFe_2O_4$  are in the form of nanoparticle, while only few studies reported on other nanostructured forms of nanowalls, aligned nanorod arrays, nanofibers and nanorods, and nanowires.  $CuFe_2O_4$  nanofibers have attracted an increasing interest in the construction of sensors and nanocomposites because of their good biocompatibility, large surface areas, super strong paramagnetic property, low toxicity, and high adsorption ability.  $CuFe_2O_4$  nanofibers can be readily separated from solution with an external magnetic field, showing great potential for heavy metal removal from water [13,14].

However, the basic disadvantages of these  $CuFe_2O_4$  nanofibers are the lack of selectivity in removal of metal ions, which leads to other species interfering with the target metal ion. Therefore, better performance of the  $CuFe_2O_4$  nanofibers can be obtained via surface modification using different types of metal oxides such as  $MnO_2$ ,  $Co_3O_4$ ,  $NiO$ ,  $TiO_2$ , and  $CeO_2$ . Cerium dioxide ( $CeO_2$ ) is one of the most active rare earth metal oxides and has been extensively used in wastewater treatment, the separation and recycling of this rare earth metal oxides like cerium oxide from the mixture is still inefficient. If the cerium oxide nanoparticles cannot be completely separated from the mixture, they will cause the secondary pollution and be not economical in applications [15,16].

In this manuscript, we have synthesized  $CuFe_2O_4$  nanofibers by combining electrospinning technique, subsequently,  $CuFe_2O_4$  nanofibers coated by  $CeO_2$  through the chemical precipitation process in order

to improve adsorption capacity ( $CeO_2/CuFe_2O_4$  nanofibers). These magnetic nanocomposites were employed as a novel adsorbent for removal of  $Pb(II)$ ,  $Ni(II)$ , and  $V(V)$  ions from water samples. The effects of contact time, solution pH, and temperature on the adsorption behavior of metal ions were investigated. Finally, kinetic and isotherm of adsorption were evaluated.

## 2. Materials and methods

### 2.1. Chemical and reagents

All chemicals were of analytical reagent grade or the highest purity available from Merck (Merck, Darmstadt, Germany). Double-distilled water was used throughout the study. Stock solutions of  $Pb(II)$ ,  $Ni(II)$ , and  $V(V)$  ( $1,000 \text{ mg L}^{-1}$ ) were prepared by dissolving appropriate amount of  $Pb(NO_3)_2$ ,  $Ni(NO_3)_2 \cdot 6H_2O$ , and  $NH_4VO_3$  in double-distilled water. Metal solutions of different initial concentrations were prepared by dilution of  $1,000 \text{ mg L}^{-1}$ . Glassware was soaked in 10% nitric acid for 12 h and rinsed three times with double-distilled water prior to use.

### 2.2. Apparatus

All pH measurements were made with a 780 pH meter (Metrohm, Switzerland) combined with a glass-calomel electrode. The crystal structure of synthesized materials was determined by an X-ray diffraction (XRD) (38066 Riva, d/G.via M. Misone, 11/D (TN) Italy) at ambient temperature. The structure of the nanoparticles was characterized by a scanning electron microscope (SEM-EDX, XL30, and Philips Netherland). Fourier transform infrared spectroscopy (FT-IR) spectra ( $4,000\text{--}400 \text{ cm}^{-1}$ ) in KBr were recorded on Perkin Elmer, spectrum100, FT-IR spectrometer. Specific surface area and porosity were defined by  $N_2$  adsorption-desorption porosimetry (77 K) using a porosimeter (Bel Japan, Inc.).

### 2.3. Sample analysis

The concentration of metal ions was determined by inductively coupled plasma optical emission spectrometry (ICP-OES) (Varian 710-ES, Australia).

### 2.4. Preparation of $CuFe_2O_4$ nanofibers

In a typical procedure, 1.0 g of poly(vinyl pyrrolidone) (PVP) was dissolved in a mixture of ethanol (9.0 ml) and double-distilled water (2.0 ml), followed

by magnetic stirring for about 5 h to ensure the dissolution of PVP. Then 1.6160 g of ferric nitrate ( $\text{Fe}(\text{NO}_3)_3 \cdot 9\text{H}_2\text{O}$ ) and 0.3993 g of copper acetate ( $\text{Cu}(\text{CH}_3\text{COO})_2 \cdot 9\text{H}_2\text{O}$ ) with the molar ratio of 2:1 were added to the above solution and magnetically stirred for about 24 h at room temperature. The solution was loaded into a plastic syringe with a stainless steel needle and the feeding speed of 0.6 ml/h was controlled by a syringe pump during the electrospinning process. While applied voltage was 17 kV between the positive and negative electrodes with the distance of 18 cm. The obtained precursor nanofibers were dried at 90°C for 20 h and subsequently calcined at 600°C with a heating rate of 2°C/min for 2 h at ambient atmosphere to form magnetic  $\text{CuFe}_2\text{O}_4$  nanofibers [17].

### 2.5. Preparation of $\text{CeO}_2$ -coated $\text{CuFe}_2\text{O}_4$ nanofibers ( $\text{CeO}_2/\text{CuFe}_2\text{O}_4$ nanofibers)

$\text{CeO}_2/\text{CuFe}_2\text{O}_4$  nanofibers were synthesized via a chemical precipitation method. First, about 0.40 g of  $\text{CuFe}_2\text{O}_4$  nanofibers and 1.0 g of  $\text{Ce}(\text{NO}_3)_3 \cdot 6\text{H}_2\text{O}$  were dispersed in double-distilled water (100 ml) and then sonicated for 30 min, followed by adding 200-ml NaOH under continuously stirring with the flow rate of 1.0 ml/min to form the precipitate. After vacuum filtration, the precipitate was washed with double-distilled water and ethanol for several times and then

dried at 120°C for 4 h. The nanocomposite was formed by calcination of the dried precipitate at 600°C for 1 h at ambient atmosphere (Fig. 1(a)).

### 2.6. Point of zero charge of the adsorbent ( $\text{pH}_{\text{PZC}}$ )

The point of zero charge (PZC) is a characteristic of metal oxides (hydroxides) and of fundamental importance in surface science. It is a concept relating to the phenomenon of adsorption and describes the condition when the electrical charge density on a surface is zero. The  $\text{pH}_{\text{PZC}}$  for the adsorbent was determined by introducing 0.005 g of adsorbent into 100-ml Erlenmeyer flasks containing 0.01 mol  $\text{L}^{-1}$   $\text{NaNO}_3$  solutions. The pH values of the solutions were adjusted between 3.0 and 8.0 using solutions of  $\text{HNO}_3$  and NaOH. The solution mixtures were allowed to equilibrate in an isothermal shaker (25°C) for 24 h. The final pH was measured after 24 h. The  $\text{pH}_{\text{PZC}}$  is the point where the  $\text{pH}_{\text{initial}} = \text{pH}_{\text{final}}$  [11].

### 2.7. Batch adsorption experiments

Metal removal experiments with 0.005 g of  $\text{CeO}_2/\text{CuFe}_2\text{O}_4$  nanofibers were performed in 25-ml stoppered conical flask containing 10 ml of metal ions solution (30 mg  $\text{L}^{-1}$ ). The pH of the solution was adjusted to 2.0–11, using 0.1 mol  $\text{L}^{-1}$  HCl and/or 0.1 mol  $\text{L}^{-1}$  NaOH solutions. The mixture was

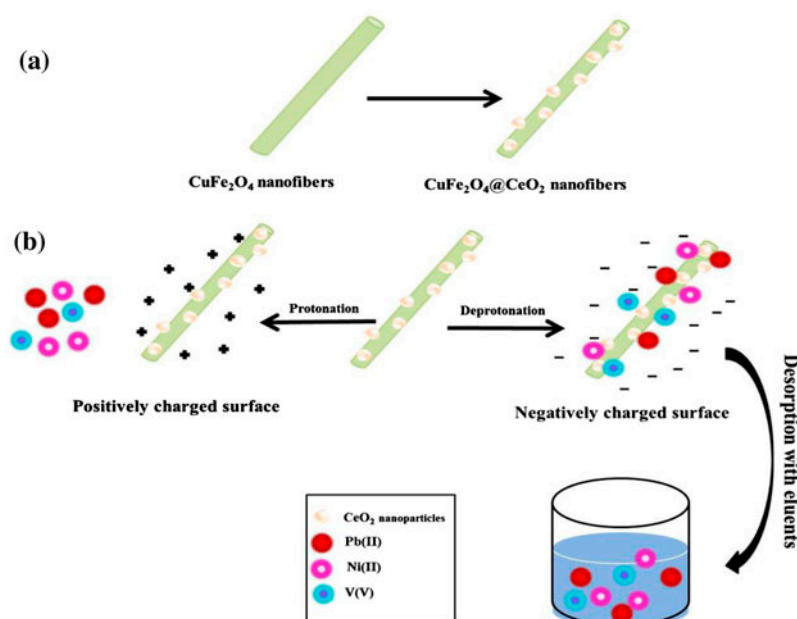


Fig. 1. Schematic diagram for (a) synthesis of the  $\text{CeO}_2/\text{CuFe}_2\text{O}_4$  nanofibers and (b) the adsorption mechanism of metal ions.

agitated in a temperature-controlled shaking water bath at a constant speed of 180 rpm. Samples were withdrawn, metal-loaded nanocomposites were separated with magnetic decantation and the concentrations of the metal ions that remained in the solution were determined by ICP-OES analysis. The metal removal efficiency was calculated using the following equation:

$$\text{Metal removal efficiency (\%)} = \frac{C_0 - C_e}{C_0} \times 100 \quad (1)$$

where  $C_0$  and  $C_e$  ( $\text{mg L}^{-1}$ ) were the initial and final metal concentrations.

Adsorption isotherm studies were carried out by adding 10 ml of different initial concentrations of Pb(II) (30–220  $\text{mg L}^{-1}$ ), Ni(II) (30–250  $\text{mg L}^{-1}$ ), and V(V) (30–250  $\text{mg L}^{-1}$ ) solution to 0.005 g of adsorbent at 25°C. The samples were shaken in a water bath shaker at 180 rpm until equilibrium was achieved. After that, the adsorbent was separated from the solution by magnetic decantation and the equilibrium concentration of metal ions in the bulk ( $C_e$ ) was determined using an ICP-OES analysis. The amount of adsorbed Pb(II), Ni(II), and V(V) ions per unit mass of adsorbent at equilibrium  $q_e$  ( $\text{mg g}^{-1}$ ), was calculated using the following equation:

$$q_e = \frac{(C_0 - C_e)V}{W} \quad (2)$$

where  $C_0$  and  $C_e$  ( $\text{mg L}^{-1}$ ) are the initial and equilibrium concentrations, respectively,  $V$  (L) is the volume of solution, and  $W$  (g) is the weight of adsorbent.

The kinetic adsorption experiments were performed at three different initial concentrations of Pb(II), Ni(II), and V(V) (30, 50, 70  $\text{mg L}^{-1}$ ). In each concentration, 10 ml of metal solution was added in to 0.005 g of adsorbent. The samples were placed in a shaker at 180 rpm at temperature 25°C and the concentration of metal ions at different time intervals ( $C_t$ ) was determined with ICP-OES analysis. The amount of adsorbed Pb(II), Ni(II), and V(V) ions per unit mass of adsorbent at different times  $q_t$  ( $\text{mg g}^{-1}$ ), was calculated using the following equation:

$$q_t = \frac{(C_0 - C_t)V}{W} \quad (3)$$

where  $C_0$  and  $C_t$  ( $\text{mg L}^{-1}$ ) are the liquid phase concentrations of Pb(II), Ni(II), and V(V) ions at initial and any time  $t$ , respectively.

## 2.8. Preparation of real samples

In order to demonstrate the applicability and reliability of the method for real samples, three samples, including tap water, river water, and petrochemical wastewater were prepared and analyzed. Tap water samples were taken from our research laboratory (Islamic Azad University, Hamedan Branch, Iran) and river water samples collected from polluted sites of the river on the Hamedan, where a cement plant is in operation nearby. River water and petrochemical wastewater were collected in a 2.0 L PTFE bottle. All samples filtered through a filter paper (Whatman No. 40) to remove suspended particulate matter.

## 3. Results and discussion

### 3.1. Characterization of adsorbents

The XRD pattern of  $\text{CuFe}_2\text{O}_4$  nanofibers (a) and  $\text{CeO}_2/\text{CuFe}_2\text{O}_4$  nanofibers (b) is shown in Fig. 2. As shown in Fig. 2(a), the XRD pattern of  $\text{CuFe}_2\text{O}_4$  nanofibers calcined at 600°C presented three intense diffraction peaks at  $2\theta$  angle of 34.718°, 35.861° and 62.156°, being well matched with the published JCPDS data (JCPDS card, file no. 34–0425) for the tetragonal  $\text{CuFe}_2\text{O}_4$ . However, a second phase of CuO ( $2\theta = 38.5^\circ$ , JCPDS card, file no. 045–0937) was also found in the calcined samples. The presence of CuO may be due to the precipitation of Cu by PVP in the solution and/or the as-spun nanofibers and then the CuO phase was formed after calcination. Compared with Fig. 1(a), after coated with  $\text{CeO}_2$  nanoparticles, the peaks of  $\text{CuFe}_2\text{O}_4$  disappear, while the diffraction peaks of  $\text{CeO}_2$  ( $2\theta = 28.68^\circ, 33.38^\circ, 47.84^\circ, 56.48^\circ, 76.86^\circ$ , and  $79.10^\circ$  (JCPDS card, file No. 34–0,394)) occur (Fig. 2(b)).

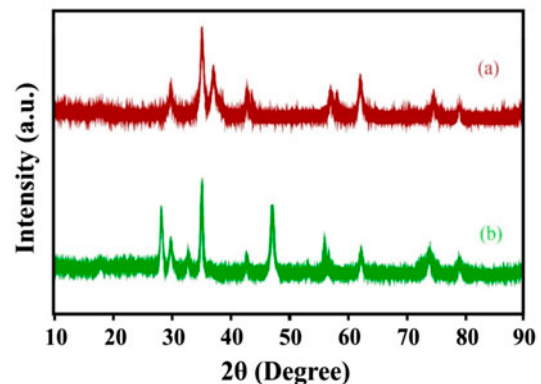


Fig. 2. XRD patterns of  $\text{CuFe}_2\text{O}_4$  nanofibers (a) and  $\text{CeO}_2/\text{CuFe}_2\text{O}_4$  nanofibers (b).

Fig. 3 shows the scanning electron microscopy (SEM) images of  $\text{CuFe}_2\text{O}_4$  nanofibers and  $\text{CeO}_2/\text{CuFe}_2\text{O}_4$  nanofibers. From these SEM images, it is obvious that the nanofibers show an average diameter of 100 nm. As shown in Fig. 3, the  $\text{CeO}_2$  nanoparticles are distributed on the orifices and surface of nanofibers. These nanofibers can effectively prevent the aggregation of nanoparticles, and the composite nanofibers band together to form abundant meso/macropores. Therefore, these porous structures will be helpful for adsorption and storage enhancement, with a high adsorption capacity of adsorbent.

The FT-IR spectra of  $\text{CeO}_2$  nanoparticles (a),  $\text{CuFe}_2\text{O}_4$  nanofibers (b) and  $\text{CeO}_2/\text{CuFe}_2\text{O}_4$  nanofibers (c) are shown in Fig. 4. The FT-IR spectra show main absorption bands at  $585\text{ cm}^{-1}$ , corresponding to the vibration modes of all spinel compounds. The ferrite can be considered as continuously bonded crystals, via ionic, covalent, or van der Waals force, to the nearest neighbors. In ferrite, the metal ions can be situated in two different sublattices, namely tetrahedral and octahedral according to the geometrical configuration of the oxygen nearest neighbor. The band around  $585\text{ cm}^{-1}$  is attributed to stretching mode of tetrahedral complexes. The absorption broad band at  $3,400\text{ cm}^{-1}$  represents the stretching mode of  $\text{H}_2\text{O}$  molecules and OH groups. The band around  $1,600\text{ cm}^{-1}$  corresponds to the bending mode of  $\text{H}_2\text{O}$  molecules (Fig. 4(b) and (c)) [15].

Specific surface areas are commonly reported as BET surface areas obtained by applying the theory of Brunauer–Emmett–Teller (BET) to nitrogen adsorption/desorption isotherms measured at 77 K. This is a standard procedure for the determination of the specific surface area of sample. The specific surface area of the sample is determined by physical adsorption of a gas onto the surface of the solid and by measuring the amount of adsorbed gas corresponding to a

monomolecular layer on the surface. The data are treated according to the BET theory [18,19]. The results of the BET method showed that the average specific surface areas of  $\text{CuFe}_2\text{O}_4$  nanofibers and  $\text{CeO}_2/\text{CuFe}_2\text{O}_4$  nanofibers were  $168.7$  and  $190.2\text{ m}^2\text{ g}^{-1}$ , respectively. It can be concluded from these values that the synthesized nanocomposite have relatively large specific surface areas. It can also be seen that the coated  $\text{CeO}_2$  nanoparticles will enhance the adsorption capacity due to a higher specific surface area and a larger amount of mesopores.

### 3.2. Adsorption isotherms

The effect of initial metal concentration on  $\text{CeO}_2/\text{CuFe}_2\text{O}_4$  nanofibers was studied at various concentrations of Pb(II), Ni(II), and V(V) solutions from 30 to  $250\text{ mg L}^{-1}$  at temperatures of  $25^\circ\text{C}$ . The results are shown in Fig. 5. As can be seen, at low initial metal ion concentrations, the available active sites on the adsorbent were rapidly occupied by metal ions. But, as the initial concentrations of Pb(II), Ni(II), and V(V) ions increased, most of the vacant available active sites became occupied. Also, the initial Pb(II), Ni(II), and V(V) concentrations provided a larger driving force to overcome the mass transfer resistance of Pb(II), Ni(II), and V(V) between the aqueous and solid phases.

Adsorption isotherms describe how different kinds of pollutants interact with adsorbents and, therefore, are very important in the clarification of adsorption mechanisms as well as in determining the equilibrium adsorption capacity and its influence on the surface properties on adsorption. Hence, adsorption isotherms are essential in the design of batch adsorption systems. In this study, the Langmuir (L), Freundlich (F), Temkin (T), Redlich–Peterson (R–P), Langmuir–Freundlich (L–F), and Brouers–Sotolongo (B–S) adsorption isotherms were used to fit the experimental data.

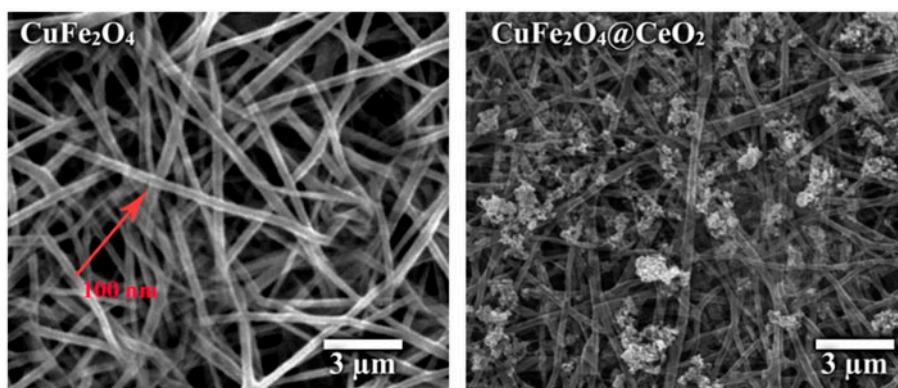


Fig. 3. SEM images of  $\text{CuFe}_2\text{O}_4$  nanofibers and  $\text{CeO}_2/\text{CuFe}_2\text{O}_4$  nanofibers.

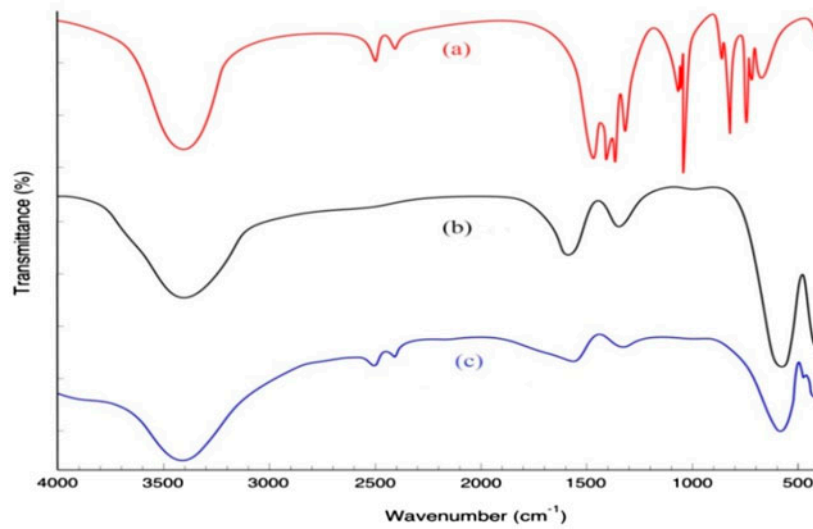


Fig. 4. FT-IR spectra of CeO<sub>2</sub> nanoparticles (a), CuFe<sub>2</sub>O<sub>4</sub> nanofibers (b), CeO<sub>2</sub>/CuFe<sub>2</sub>O<sub>4</sub> nanofibers (c).

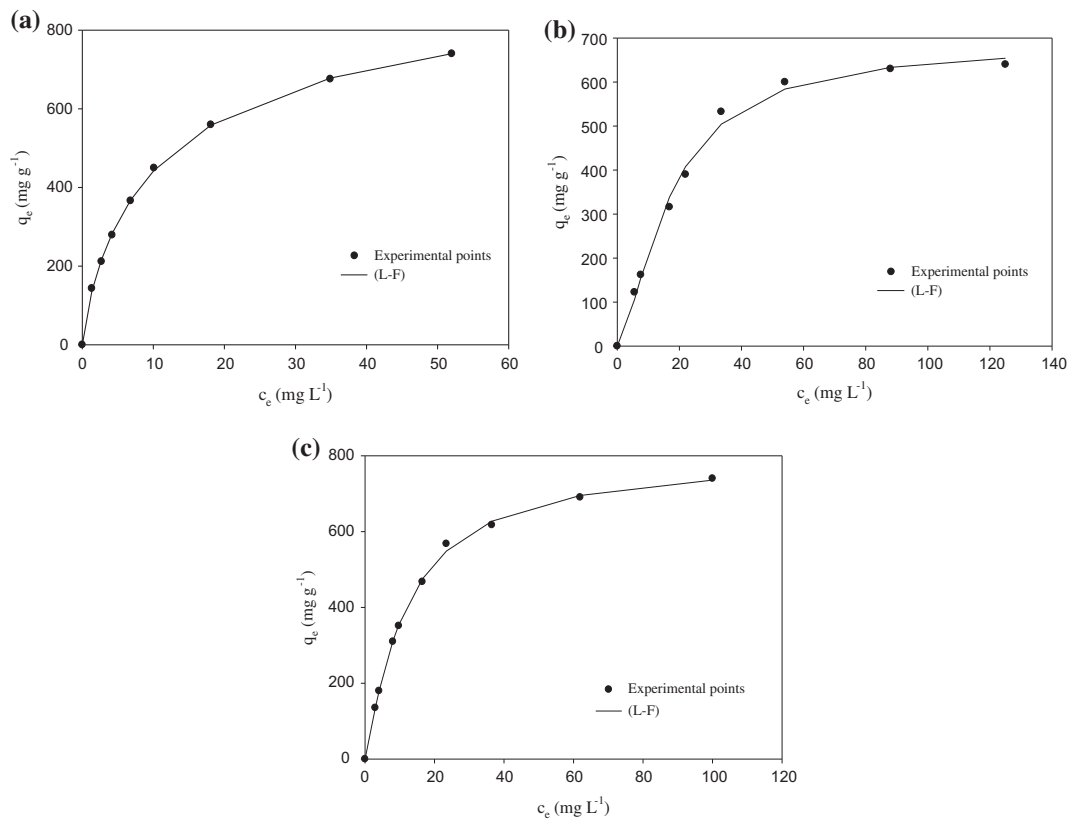


Fig. 5. Adsorption isotherm of (a) Pb(II), (b) Ni(II), and (c) V(V) onto CeO<sub>2</sub>/CuFe<sub>2</sub>O<sub>4</sub> nanofibers.

Langmuir isotherm is often used to describe adsorption of solute from liquid solutions and this model assumes monolayer adsorption onto a homoge-

neous surface with finite number of identical sites [20]. The non-linear form of Langmuir isotherm model is given as follows:

$$q_e = \frac{q_m K_L C_e}{1 + K_L C_e} \quad (4)$$

where  $q_m$  ( $\text{mg g}^{-1}$ ) and  $K_L$  ( $\text{L mg}^{-1}$ ) are known as Langmuir constants and referred to maximum adsorption capacity and affinity of adsorption, respectively. In order to predict the favorability of the adsorption process, the essential characteristic of Langmuir equation can be described using the dimensionless separation factor  $R_L$ , which can be defined as follows:

$$R_L = \frac{1}{1 + K_L C_0} \quad (5)$$

where  $C_0$  is the maximal initial concentration of metal ion ( $\text{mg L}^{-1}$ ).  $R_L$  indicates that the nature of the adsorption process. If  $R_L > 1$ , the isotherm is unfavorable,  $R_L = 1$ , the isotherm is linear,  $0 < R_L < 1$ , the isotherm is favorable,  $R_L = 0$ , the isotherm is irreversible.

The Freundlich model assumes that the uptake or adsorption of solute occurs on the heterogeneous surface [21]. The non-linear form of Freundlich isotherm presented as follows:

$$q_e = K_F (C_e)^{1/n} \quad (6)$$

where  $K_F$  ( $\text{mg}^{1-(1/n)} \text{L}^{1/n} / \text{g}$ ) is Freundlich constant and  $n$  indicating adsorption heterogeneity.

The Temkin isotherm shows the effects of indirect interactions between adsorbate molecules based on the assumption that the heat of adsorption of all molecules in the layer would decrease linearly with surface coverage [22]. Temkin isotherm model is:

$$q_e = B \ln(AC_e) \quad (7)$$

where  $B = RT/b$  and  $b$  ( $\text{J mol}^{-1}$ ) is the Temkin constant related to the heat of adsorption;  $A$  ( $\text{L mg}^{-1}$ ) is the Temkin isotherm constant.

Redlich and Peterson (R-P) proposed an isotherm compromising the features of the Langmuir and the Freundlich isotherms. Redlich–Peterson is one of the three-parameter equations [23]:

$$q_e = \frac{k_{R-P} C_e}{1 + \alpha C_e^\beta} \quad (8)$$

where  $k_{R-P}$  ( $\text{L g}^{-1}$ ),  $\alpha$ ,  $\beta$  are the Redlich–Peterson constants.  $\beta$  is the parameter which is between 0 and 1.

The other isotherm model used for modeling of equilibrium adsorption data is Langmuir–Freundlich

isotherm. The Langmuir–Freundlich isotherm model is obtained by introducing a power law expression of the Freundlich isotherm into the Langmuir isotherm. At low adsorbate concentrations, it reduces to Freundlich isotherm; while at high concentrations, it predicts a monolayer adsorption capacity characteristic of the Langmuir isotherm [24]:

$$q_e = \frac{q_m (K_{L-F} C_e)^{1/n}}{1 + (K_{L-F} C_e)^{1/n}} \quad (9)$$

where  $K_{L-F}$  ( $\text{L mg}^{-1}$ ) and  $n$  are constants.

Brouers–Sotolongo proposed an isotherm for heterogeneous surface containing micro cores [25]. Its expression is given as follows:

$$q_e = q_m (1 - \exp(-k_{B-S} C_e^a)) \quad (10)$$

where  $q_m$  is the maximum adsorption capacity,  $C_e$  and  $k_{B-S}$  are equilibrium concentration ( $\text{mg L}^{-1}$ ) and Brouers–Sotolongo isotherm constant, respectively. The exponent is a measure of the width of the adsorption energy distribution and therefore of the energy heterogeneity of the adsorbent surface.

Fitting parameters for the Langmuir, Freundlich, Temkin, Redlich–Peterson, Langmuir–Freundlich, and Brouers–Sotolongo (B–S) isotherm models are listed in Table 1. It was found that higher correlation coefficients value ( $r^2 = 0.990$  for Pb(II),  $r^2 = 0.992$  for Ni(II), and  $r^2 = 0.991$  for V(V)) and smaller RMS error value of Langmuir–Freundlich isotherm compared to the similar value of other applied model confirm the high efficiency of Langmuir–Freundlich isotherm to represent the experimental data. This means that adsorbent provides a heterogeneous surface, i.e. there are different active sites for adsorption. The results of fitting by this isotherm are shown in Fig. 5. The obtained maximum adsorption capacities for Pb(II), Ni(II), and V(V) ions on the  $\text{CeO}_2/\text{CuFe}_2\text{O}_4$  nanofibers are 972.4, 686.1, and 798.6  $\text{mg g}^{-1}$ , respectively. Adsorption capacity increased in the sequence of  $\text{Pb(II)} > \text{V(V)} > \text{Ni(II)}$ , where the different adsorption capacities may be due to disparity in cations radius and interaction enthalpy values. The adsorption capacities of different types of adsorbents for Pb(II), Ni(II), and V(V) ions are summarized in Table 2. It is evident that the  $\text{CeO}_2/\text{CuFe}_2\text{O}_4$  nanofibers used in this work have a larger adsorption capacity than many reported adsorbents.

Based on the results described, we propose that two adsorption mechanisms may be involved in the process of Pb(II), Ni(II), and V(V) ions adsorption on  $\text{CeO}_2/\text{CuFe}_2\text{O}_4$  nanofibers: chemical binding

Table 1  
Obtained parameters for adsorption of metal ions onto  
CeO<sub>2</sub>/CuFe<sub>2</sub>O<sub>4</sub> nanofibers

Isotherm	Parameters	Metal cations		
		Pb(II)	Ni(II)	V(V)
L	$q_m$ (mg g <sup>-1</sup> )	860.9	807.69	850.9
	$K_L$ (L mg <sup>-1</sup> )	0.111	0.042	0.072
	$R_L$	0.300	0.793	0.462
	$r^2$	0.9957	0.9701	0.9960
	RMS error	11.566	38.892	15.826
F	$K_F$ (L mg <sup>(1-(1/n))</sup> /g)	174.5	105.89	150.3
	$n$	0.368	0.397	0.366
	$r^2$	0.9729	0.8730	0.9172
	RMS error	41.06	80.278	67.515
T	$B$	171.5	183.5	181.79
	$A$ (L mg <sup>-1</sup> )	1.383	0.368	0.734
	$r^2$	0.9970	0.9575	0.9859
	RMS error	8.231	46.389	27.788
B-S	$q_m$ (mg g <sup>-1</sup> )	814.4	638.8	729.1
	$a$	0.692	1.180	0.886
	$K_{B-S}$ (L mg <sup>-1</sup> ) <sup>a</sup>	0.156	0.025	0.085
	$r^2$	0.9958	0.9894	0.9964
L-F	RMS error	11.231	15.520	14.517
	$q_m$ (mg g <sup>-1</sup> )	972.4	686.1	798.6
	$K_{L-F}$ (L mg <sup>-1</sup> )	0.079	0.058	0.084
	$n$	1.227	0.659	0.867
R-P	$r^2$	0.9982	0.9920	0.9974
	RMS error	7.765	12.520	9.826
	$K_{R-P}$ (L g <sup>-1</sup> )	125.1	23.14	54.76
	$\alpha'$ (L mg <sup>-1</sup> ) <sup>1/β</sup>	0.236	0.003	0.044
	$B$	0.884	1.453	1.083
	$r^2$	0.9962	0.9861	0.9969
	RMS error	10.221	16.301	14.121

adsorption and electrostatic binding adsorption. Considering the presence of H<sup>+</sup> (from hydroxyl group) or Na<sup>+</sup> on the surface of CeO<sub>2</sub>/CuFe<sub>2</sub>O<sub>4</sub> nanofibers, it was believed that Pb(II), Ni(II), and V(V) ions could exchange with H<sup>+</sup> ions or Na<sup>+</sup> ions and then bonded with O atoms. Meanwhile, the negative charged CeO<sub>2</sub>/CuFe<sub>2</sub>O<sub>4</sub> nanofibers with deprotonated hydroxyl groups had an electrostatic attractive interaction with Pb(II), Ni(II), and V(V) ions (Fig. 1(b)). Similar adsorption mechanisms were also proposed by SDS-coated magnetite nanoparticles modified with 2,4-DNPH [26] and zinc oxide nanoparticles (ZnO) [27].

### 3.3. Adsorption kinetics

The effect of contact time on the adsorption capacity of CeO<sub>2</sub>/CuFe<sub>2</sub>O<sub>4</sub> nanofibers for removal of Pb(II), Ni(II), and V(V) ions was carried out at temperature 25°C and initial metal concentration of 30 mg L<sup>-1</sup>. As shown in Fig. 6, the adsorption equilibrium for Pb(II), Ni(II), and V(V) ions was fast and was achieved within 70 min. Generally, the adsorption of Pb(II), Ni(II), and V(V) ions by CeO<sub>2</sub>/CuFe<sub>2</sub>O<sub>4</sub> nanofibers showed two stages: a rapid adsorption stage of the first 40 min, and a slower stage of 40–70 min. At the start of the adsorption, metal ions removal can be rapid surface adsorption (external surface adsorption). In the later slower stage, adsorption mainly occurred via transportation of surface-adsorbed metal ions to the internal adsorption sites of the adsorbent (internal surface adsorption). Meanwhile, part of external sites were released and cycled for next adsorption. After 70 min, the adsorption reached equilibrium.

Table 2  
Comparison of maximum adsorption capacity ( $q_m$ ) of different adsorbents for Pb(II), Ni(II), and V(V)

Adsorbent	Maximum adsorption capacity (mg g <sup>-1</sup> )			Refs.
	Pb(II)	Ni(II)	V(V)	
Amine-functionalized mesoporous Fe <sub>3</sub> O <sub>4</sub> nanoparticles	369	–	–	[28]
Oxidized multi-walled carbon nanotubes	–	–	100	[29]
Magnetic $\gamma$ -Fe <sub>2</sub> O <sub>3</sub> /titanate nanotubes composite	223.7	–	–	[30]
Chitosan-zirconium (IV) composite	–	–	208	[6]
EDTA functionalized magnetic graphene oxide	508.4	–	–	[31]
Thiol modified Fe <sub>3</sub> O <sub>4</sub> @SiO <sub>2</sub>	–	148.8	–	[32]
Al(OH) <sub>3</sub> /(PAA-CO-PAM) sub-microspheres	106.2	–	–	[33]
Protonated chitosan flakes	–	–	2.58	[34]
Chitosan-modified poly(methacrylate) nanoparticles	–	340	–	[35]
Mg–Al layered double hydroxides/MnO <sub>2</sub>	49.87	–	–	[36]
CeO <sub>2</sub> /CuFe <sub>2</sub> O <sub>4</sub> nanofibers	972.4	686.1	798.6	This work

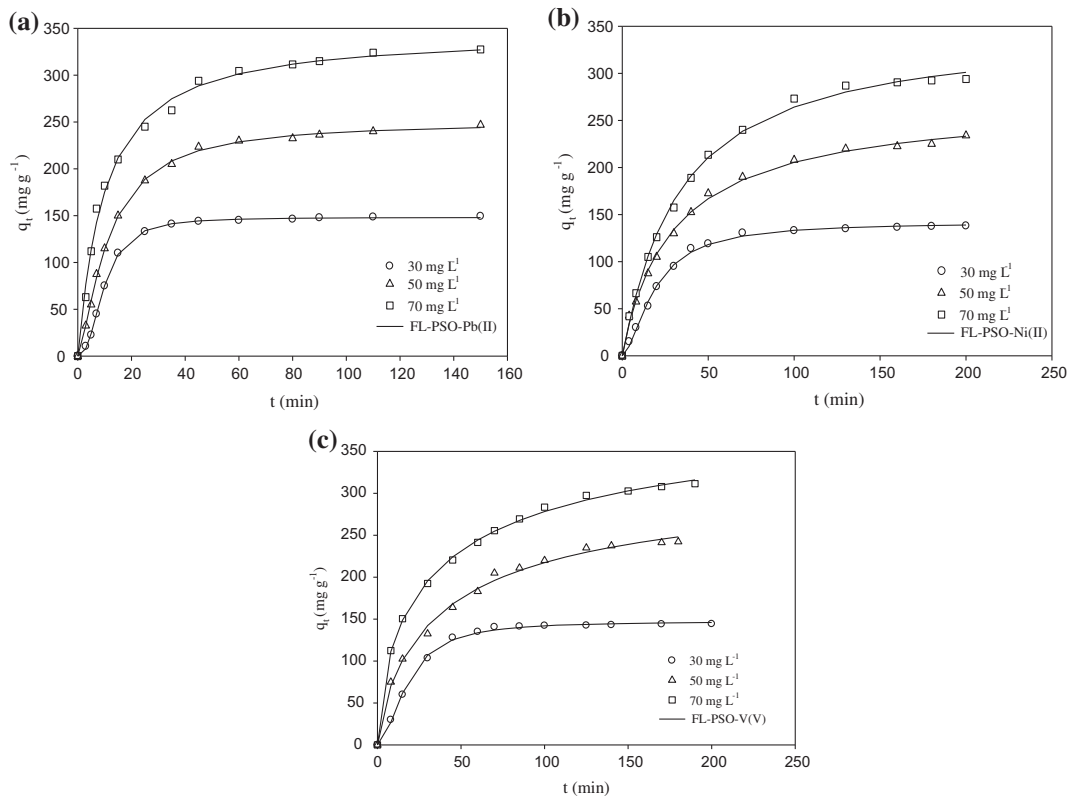


Fig. 6. Experimental kinetic data for the adsorption of (a) Pb(II), (b) Ni(II), and (c) V(V) by CeO<sub>2</sub>/CuFe<sub>2</sub>O<sub>4</sub> nanofibers at different initial concentrations. Lines represent the FL-PSO model fitted to the data.

Kinetic models are a significant aspect of adsorption studies and define the efficiency of the adsorption process. Kinetic models are proposed for a better understanding of the mechanism of adsorption. In order to investigate the adsorption behaviors of Pb(II), Ni(II), and V(V) ions with the adsorbent, six kinetic models (pseudo-first-order (PFO), pseudo-second-order (PSO), Elovich (E), mixed 1,2-order (MOE), Exponential (EXP) and fractal-like pseudo-second-order (FL-PSO)) have been employed to simulate the experimental data by non-linear method.

Pseudo-first-order equation is one of the most popular and empirical models for adsorption kinetics which presented by Lagergren [37]. The integrated form of this model can be given as follows:

$$q_t = q_e(1 - \exp(-k_1 t)) \tag{11}$$

where  $q_t$  and  $q_e$  (mg g<sup>-1</sup>) are the amount of adsorbed species per unit mass of adsorbent at any time ( $t$ ) and at equilibrium, respectively.  $k_1$  (min<sup>-1</sup>) is the pseudo-first-order rate constant.

Another simple and well-known kinetic model which is used extensively in recent years is pseudo-

second-order equation [37]. The integrated form of this equation is:

$$q_t = \frac{k_2 q_e^2 t}{1 + k_2 q_e t} \tag{12}$$

where  $k_2$  (g mg<sup>-1</sup> min) is the rate coefficient.

The mixed 1,2-order, that is the combination of first- and second-order equations, is expressed by [38]:

$$q_t = q_e \frac{1 - \exp(-k_1 t)}{1 - F_2 \exp(-k_1 t)} \tag{13}$$

where  $F_2$  ( $F_2 < 1$ ) is determining the share of second-order term in the order rate equation.

$$F_2 = \frac{k_2 q_e}{k_1 + k_2 q_e}, \quad F_1 + F_2 = 1 \tag{14}$$

In order to investigate the adsorption of pollutants from aqueous solution, Elovich rate equation has been widely used [39]. The integrated form of Elovich equation is expressed as follows:

$$q_t = \frac{1}{a} \ln(1 + abt) \quad (15)$$

where  $a$  and  $b$  are equation constants. Mainly, Elovich equation is applied to describe chemical adsorption onto heterogeneous adsorbent surfaces.

Exponential model is one of the new empirical models which are suitable for modeling of adsorption kinetic onto both homogeneous and heterogeneous solid surfaces [40]. Its integrated form is:

$$q_t = q_e \ln[2.72 - 1.72] \exp(-k'_1 t) \quad (16)$$

where  $k'_1$  is constant.

One of the recently developed kinetic models for adsorption is the fractal-like pseudo second-order model, which was presented for the systems with different paths of adsorption [41]. The integrated form of this equation is:

$$q_t = \frac{k'_2 q_e^2 t^x}{1 + k'_2 q_e t^x} \quad (17)$$

where  $k'_2$  is a constant.

The parameters obtained by non-linear fitting using different kinetic models were summarized in Table 3. Based on correlation coefficient values ( $r^2 > 0.99$ ) and the RMS error value, the FL-PSO kinetic model agreed well with the adsorption of Pb(II), Ni(II), and V(V) ions onto CeO<sub>2</sub>/CuFe<sub>2</sub>O<sub>4</sub> nanofibers. Following of kinetic data by this model means that the adsorption sites changes with time due to surface heterogeneity of adsorbent. Comparison of  $\alpha$  value of the FL-PSO model at different concentrations indicates a small increase in  $\alpha$  with concentration and approaching to unity. This means that by increasing the concentration the number of paths for adsorption decreases, and at high concentrations the adsorbates are directly adsorbed onto active sites. In addition, the obtained  $q_{e(\text{cal})}$  values by FL-PSO model matched well with the experimental  $q_{e(\text{exp})}$ . The results of fitting by the FL-PSO models are shown by solid lines in Fig. 6.

### 3.4. Effect of solution pH

pH of the solution in the adsorption process of metal molecules can affect both aqueous chemistry and surface-binding sites of the adsorbent. The effect of the pH on the removal efficiency of Pb(II), Ni(II), and V(V) ions was studied in the pH range from 2.0 to 11 for initial metal ion concentration of 30 mg L<sup>-1</sup>. As shown in Fig. 7, the maximum removal efficiencies

were obtained at pH of 7.0 for Pb(II), Ni(II), and 6.0 for V(V), with the values of 99.4, 92.5, and 94.5%, respectively.

The adsorption curve of Pb(II), Ni(II), and V(V) ions onto CeO<sub>2</sub>/CuFe<sub>2</sub>O<sub>4</sub> nanofibers can be divided into three regions. In the first region (pH 2.0–6.0), the adsorption efficiency of Pb(II), Ni(II), and V(V) ions sharply increases when the pH increases from 2.0 to 6.0. In the second region, when the pH values increase from 6.0 to 8.0, the corresponding adsorption efficiency has no obvious change and nearly maintains the maximum value. When the pH is above 8.0, the removal of Pb(II), Ni(II), and V(V) ions gradually decreases along with the increase in the pH values (third region). The variations of adsorption efficiency can be attributed to the different interactions between the CeO<sub>2</sub>/CuFe<sub>2</sub>O<sub>4</sub> nanofibers and the metal ions. The solution pH not only has great influence on the surface properties of the CeO<sub>2</sub>/CuFe<sub>2</sub>O<sub>4</sub> nanofibers, but also exerts tremendous effect on the existing forms of Pb(II), Ni(II) and V(V) ions. As for CeO<sub>2</sub>/CuFe<sub>2</sub>O<sub>4</sub> nanofibers, the effects of pH can be summarized into two aspects: the change of surface charges and the dissociation of –OH groups. According to the zeta potential test, the pH<sub>pzc</sub> for the synthesized CeO<sub>2</sub>/CuFe<sub>2</sub>O<sub>4</sub> nanofibers is determined to be 4.5 and this means that the surfaces will be positively charged when the solution pH is below 4.5. The surfaces of CeO<sub>2</sub>/CuFe<sub>2</sub>O<sub>4</sub> nanofibers will become negatively charged when the pH is above 4.5. Meanwhile, the surface of CeO<sub>2</sub>/CuFe<sub>2</sub>O<sub>4</sub> nanofibers contains a large number of binding sites and may become positively charged at low pH values because of the protonation reaction on the surfaces (–ROH<sub>(surf)</sub> + H<sub>(aq)</sub><sup>+3/4</sup> ROH<sub>2(surf)</sub><sup>+</sup>). As the pH of solution increases, the surfaces of CeO<sub>2</sub>/CuFe<sub>2</sub>O<sub>4</sub> nanofibers will become negatively charged because of the deprotonation reaction on the surfaces (–ROH<sub>(surf)</sub> + OH<sub>(aq)</sub><sup>-3/4</sup> –RO<sub>(surf)</sub><sup>-</sup> + H<sub>2</sub>O).

When the pH is low (pH < 4.5), the surfaces of the CeO<sub>2</sub>/CuFe<sub>2</sub>O<sub>4</sub> nanofibers are positively charged. Under this condition, an electrostatic repulsion force will exist between the metal ions and CeO<sub>2</sub>/CuFe<sub>2</sub>O<sub>4</sub> nanofibers, preventing from Pb(II), Ni(II), and V(V) adsorption onto the surface of CeO<sub>2</sub>/CuFe<sub>2</sub>O<sub>4</sub> nanofibers. While the pH value increases (pH > 4.5), the surfaces of CeO<sub>2</sub>/CuFe<sub>2</sub>O<sub>4</sub> nanofibers became less positively charged, leading to the decrease in electrostatic repulsion force, which will facilitate the adsorption of Pb(II), Ni(II), and V(V) ions onto CeO<sub>2</sub>/CuFe<sub>2</sub>O<sub>4</sub> nanofibers, resulting in the increase in adsorption efficiency in the first region. In the second region (pH 6.0–8.0), the removal of Pb(II), Ni(II), and V(V) ions is possible to be accomplished by the precipitation and simultaneous adsorption.

Table 3  
Constant of kinetic models for adsorption of metal ions onto CeO<sub>2</sub>/CuFe<sub>2</sub>O<sub>4</sub> nanofibers

Isotherm	Parameters	Metal cations								
		Pb(II)			Ni(II)			V(V)		
		30	50	70	30	50	70	30	50	70
PFO	$k_1$ (min <sup>-1</sup> )	0.066	0.061	0.080	0.037	0.030	0.026	0.039	0.028	0.036
	$q_e$ (mg g <sup>-1</sup> )	150.6	238.6	309.4	138.1	224.4	293.2	145.9	237.8	294.9
	$r^2$	0.9722	0.9964	0.9804	0.9949	0.9915	0.9966	0.9929	0.9787	0.9621
	RMS error	10.052	5.356	15.362	3.687	7.358	6.176	4.354	11.49	18.74
PSO	$k_2$ (g mg <sup>-1</sup> min)	0.000	0.000	0.000	0.000	0.005	0.020	0.000	0.000	0.000
	$q_e$ (mg g <sup>-1</sup> )	175.9	278.9	351.8	161.4	266.3	354.6	170.3	283.3	340.2
	$r^2$	0.9427	0.9889	0.9947	0.9772	0.9972	0.9973	0.9678	0.9920	0.9912
	RMS error	14.440	9.459	7.985	7.850	4.224	5.481	9.272	7.045	8.992
E	$a$	0.025	0.016	0.014	0.027	0.016	0.011	0.027	0.015	0.014
	$b$	20.62	32.63	73.70	11.689	15.145	15.638	15.49	17.32	36.29
	$r^2$	0.8892	0.9571	0.9741	0.8504	0.8963	0.9722	0.9221	0.9927	0.9976
	RMS error	20.079	18.617	17.673	12.70	7.999	11.63	14.42	6.717	4.622
EXP	$k'_1$	0.034	0.031	0.024	0.025	0.020	0.018	0.027	0.020	0.025
	$q_e$ (mg g <sup>-1</sup> )	153.3	243.4	270.26	140.4	229.5	301.2	148.3	243.7	300.8
	$r^2$	0.9598	0.9948	0.9890	0.9881	0.9963	0.9980	0.9839	0.9881	0.9787
	RMS error	12.092	6.422	11.483	5.655	4.832	5.557	6.554	8.580	14.06
MOE	$F_2$	7.963	0.068	0.911	1.059	0.781	2.144	1.453	0.978	0.999
	$k_1$ (min <sup>-1</sup> )	0.225	0.058	0.022	0.058	0.007	0.016	0.067	0.000	0.001
	$q_e$ (mg g <sup>-1</sup> )	145.1	239.1	338.6	135.9	244.2	650.1	143.1	288.8	347.4
	$r^2$	0.9961	0.9964	0.9947	0.9982	0.9972	0.9985	0.9995	0.9913	0.9899
	RMS error	3.892	5.570	8.331	2.835	4.354	4.216	1.131	7.706	10.13
FL-PSO	$\alpha$	0.521	0.737	1.215	0.225	0.218	0.754	0.356	0.434	0.915
	$k'_2$	0.000	0.000	0.001	0.000	0.000	0.000	0.001	0.000	0.010
	$q_e$ (mg g <sup>-1</sup> )	147.0	238.5	334.0	135.2	228.0	300.2	144.5	242.4	318.5
	$r^2$	0.9996	0.9991	0.9950	0.9987	0.9979	0.9987	0.9980	0.9951	0.9988
	RMS error	1.254	2.808	8.089	1.938	3.982	3.793	2.423	5.739	3.347
Experimental data	$q_{e(\text{exp})}$	145.0	236.0	324.0	133.0	222.5	290.5	141.5	237.5	302.7

In the third region (pH 9.0–11), the hydrolyzed species, such as Pb(OH)<sub>2</sub><sup>0</sup>, Pb(OH)<sub>3</sub><sup>-</sup>, Ni(OH)<sub>3</sub><sup>-</sup>, Ni(OH)<sub>4</sub><sup>2-</sup>, V<sub>3</sub>O<sub>9</sub><sup>3-</sup>, HVO<sub>4</sub><sup>2-</sup>, and HV<sub>2</sub>O<sub>7</sub><sup>3-</sup> gradually increase and become the primary species. Therefore, the decrease in the removal percentage might be ascribed to the reason that the complexation between metal ions and CeO<sub>2</sub>/CuFe<sub>2</sub>O<sub>4</sub> nanofibers is weakened and the difficulty in the adsorption of these species onto the negatively charged surface.

### 3.5. Effect of temperature

Temperature mainly influences metal ion adsorption by affecting the chemical structure of an adsorbent surface, as well as the physical and chemical status of a solution. Therefore, controlling the adsorption temperature is necessary to achieve the optimal adsorption. In order to determine the effect of temperature on the removal of Pb(II), Ni(II), and V(V) ions by CeO<sub>2</sub>/CuFe<sub>2</sub>O<sub>4</sub> nanofibers, adsorption experi-

ments were tested at four temperatures (25, 35, 45, and 55 °C). Fig. 8 shows the removal percentage of Pb(II) and Ni(II) ions are found to enhance from 92.2 to 99.7 and 82.9 to 95.1, respectively, with rising temperature from 25 to 55 °C. The results show that a better adsorption performance could be obtained at a higher temperature and higher temperature facilitates to adsorption of metal ions. Therefore, the adsorption of these metals onto CeO<sub>2</sub>/CuFe<sub>2</sub>O<sub>4</sub> nanofibers is endothermic. This may result in increasing mobility of metal ions and number of active sites on CeO<sub>2</sub>/CuFe<sub>2</sub>O<sub>4</sub> nanofibers for the adsorption with increased temperature. Similar results for the metal ions adsorption at various temperatures on graphene oxide [5] and Chitosan-modified poly(methacrylate) nanoparticles [35] have also been reported. Fig. 8 shows that the removal percentage of V(V) ions by CeO<sub>2</sub>/CuFe<sub>2</sub>O<sub>4</sub> nanofibers has been decreased with increasing temperature. By increasing temperature from 25 to 55 °C, the removal percentage of V(V)

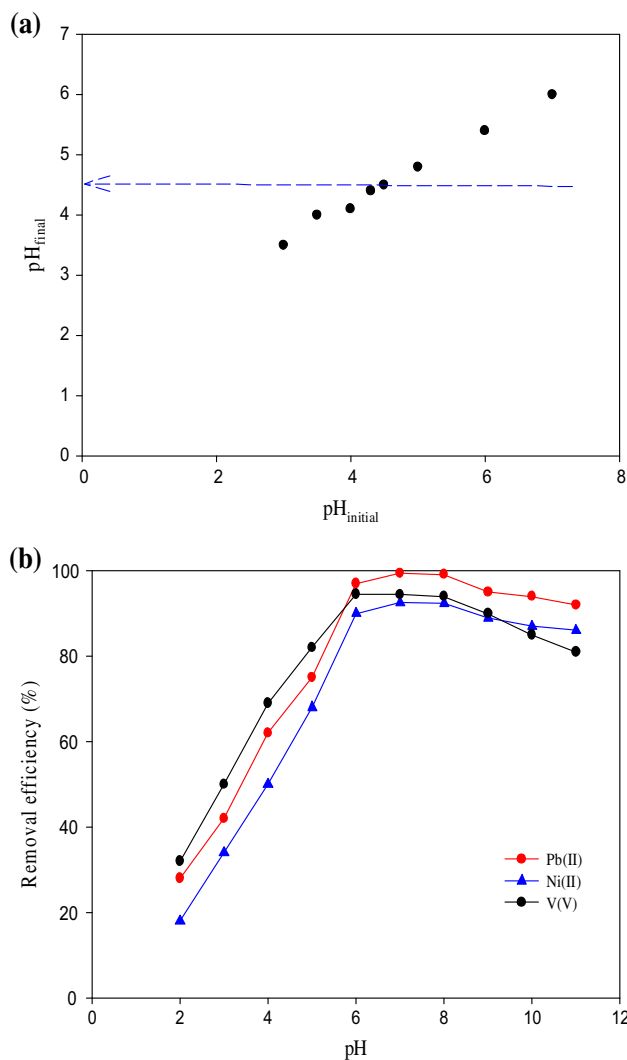


Fig. 7. (a) pH variation in terms of initial pH of solution for determination of PZC pH. (b) Effect of solution pH on the removal percentage of metal ions by CeO<sub>2</sub>/CuFe<sub>2</sub>O<sub>4</sub> nanofibers.

decrease from 98.3 to 78.5. These result indicate that the adsorption of V(V) ions by CeO<sub>2</sub>/CuFe<sub>2</sub>O<sub>4</sub> nanofibers is an exothermic process.

### 3.6. Desorption and reusability

The stability and reusability of an adsorbent during adsorption/desorption cycles are important factors in designing large-scale applications from the environmental and economic points of view. The metals adsorbed on the surface of adsorbents can be recovered by desorption with adequate eluents. In order to obtain the optimum desorption performance, desorption experiments were performed under batch

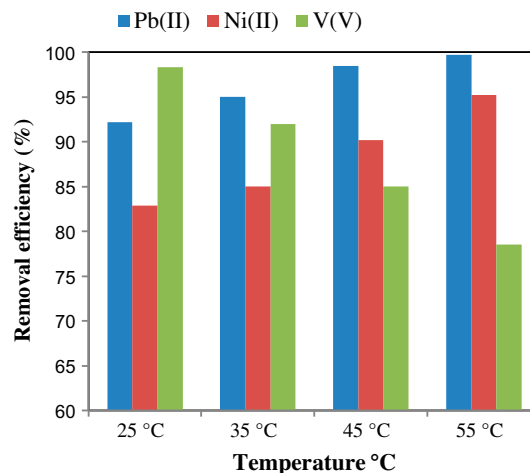


Fig. 8. Effect of temperature on the removal percentage of metal ions by CeO<sub>2</sub>/CuFe<sub>2</sub>O<sub>4</sub> nanofibers.

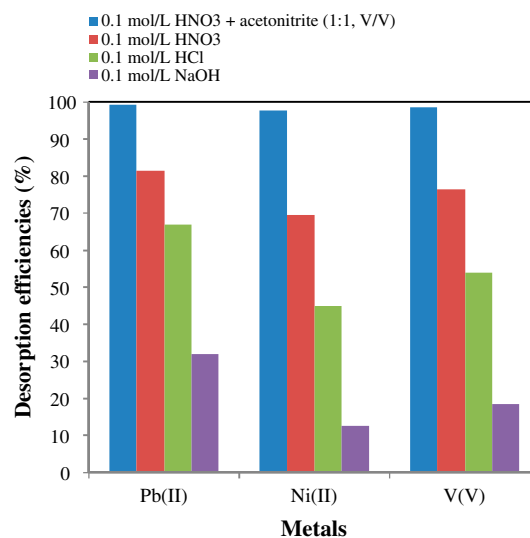


Fig. 9. Effect of type of eluting agent on recovery (%) for metal ions adsorbed onto CeO<sub>2</sub>/CuFe<sub>2</sub>O<sub>4</sub> nanofibers.

experimental conditions. In this study, desorption of Pb(II), Ni(II), and V(V) from the adsorbent has been done with various effluents such as 0.1 mol L<sup>-1</sup> NaOH, 0.1 mol L<sup>-1</sup> HNO<sub>3</sub>, 0.1 mol L<sup>-1</sup> HCl, and 0.1 mol L<sup>-1</sup> HNO<sub>3</sub> + acetonitrile (1:1, V/V). Desorption process was performed on loaded nanocomposite by mixing loaded CeO<sub>2</sub>/CuFe<sub>2</sub>O<sub>4</sub> nanofibers with 5 mL of different eluents in a beaker. The mixture was shaken for 10, 15, 30, 40, and 50 min to reach desorption equilibrium and nanocomposite were collected magnetically from the solution. Then the concentration of metals in the desorbed solution was measured by

Table 4  
Results of adsorption of metal ions in various water samples under the optimum conditions ( $n = 3$ )

Sample	Metals	Added ( $\mu\text{g L}^{-1}$ )	Found ( $\mu\text{g L}^{-1}$ )	Recovery (%)
Tap water	Pb(II)	30	29.8	99.3
		60	59.9	99.8
	Ni(II)	30	28.9	96.3
		60	60.1	100.1
	V(V)	30	29.5	98.3
		60	59.1	98.5
River water	Pb(II)	30	30.2	100.6
		60	59.6	99.3
	Ni(II)	30	29.2	97.3
		60	58.1	96.8
	V(V)	30	30.1	100.3
		60	58.9	98.1
Petrochemical wastewater	Pb(II)	30	29.2	97.3
		60	58.8	98.5
	Ni(II)	30	28.5	95.5
		60	53	88.3
	V(V)	30	27.5	91.6
		60	56.5	94.1

ICP-OES. The results for the metal ions desorption are given in Fig. 9. As the results show, the desorption efficiencies for mixture of acetonitrile with  $0.1 \text{ mol L}^{-1}$   $\text{HNO}_3$  were higher than other solutions at desorption time of 30 min. Also, the results shown that after five cycles, the recovery efficiencies of metal ions still maintain above 94%, which indicate that the adsorbent had excellent stability and reusability.

### 3.7. Adsorption of Pb(II), Ni(II), and V(V) ions in real samples

The applicability of the prepared  $\text{CeO}_2/\text{CuFe}_2\text{O}_4$  nanofibers was tested by adsorption of Pb(II), Ni(II), and V(V) ions in tap water, river water, and petrochemical wastewater. The results presented in Table 4 indicated that  $\text{CeO}_2/\text{CuFe}_2\text{O}_4$  nanofibers its efficiency for the adsorption of Pb(II), Ni(II), and V(V) ions in various samples with satisfactory results. Besides, the recovery studies of the spiked metal ions in samples showed average recovery of 99.1 for Pb(II), 95.5 for Ni (II), and 96.8 for V(V), respectively (Table 4), suggesting the applicability of successful of the proposed method for the wastewater treatment.

## 4. Conclusion

In summary, the  $\text{CeO}_2/\text{CuFe}_2\text{O}_4$  nanocomposite has been fabricated via a new facile route. We showed that  $\text{CeO}_2/\text{CuFe}_2\text{O}_4$  nanocomposite could be used as a suitable adsorbent for removal of metal ions from

water samples. The maximum removal efficiency by  $\text{CeO}_2/\text{CuFe}_2\text{O}_4$  nanofibers is at pH 7.0 for Pb(II), Ni (II), and pH 6.0 for V(V). The kinetic studies reveal that the rate of adsorption onto  $\text{CeO}_2/\text{CuFe}_2\text{O}_4$  nanofibers is rapid i.e. the paths of adsorption changes with time and obtained data follow FL-PSO model. Also, the results of equilibrium studies show that the equilibrium data follow the Langmuir–Freundlich isotherm which indicates that adsorbent has a heterogeneous surface. Furthermore, simple and fast magnetic recycling of the nanocomposite through the application of an external magnetic field was taken into account as an advantage.

## References

- [1] M. Ceglowski, G. Schroeder, Preparation of porous resin with Schiff base chelating groups for removal of heavy metal ions from aqueous solutions, *Chem. Eng. J.* 263 (2015) 402–411.
- [2] Y. Meng, D. Chen, Y. Sun, D. Jiao, D. Zeng, Z. Liu, Adsorption of  $\text{Cu}^{2+}$  ions using chitosan-modified magnetic Mn ferrite nanoparticles synthesized by microwave-assisted hydrothermal method, *Appl. Surf. Sci.* 324 (2015) 745–750.
- [3] L. Jiang, P. Liu, S. Zhao, Magnetic ATP/FA/Poly(AA-co-AM) ternary nanocomposite microgel as selective adsorbent for removal of heavy metals from wastewater, *Colloids Surf., A* 470 (2015) 31–38.
- [4] M. Li, M.-Y. Li, C.-G. Feng, Q.-X. Zeng, Preparation and characterization of multi-carboxyl-functionalized silica gel for removal of Cu (II), Cd (II), Ni (II) and Zn (II) from aqueous solution, *Appl. Surf. Sci.* 314 (2014) 1063–1069.

- [5] X. Huang, M. Pan, The highly efficient adsorption of Pb(II) on graphene oxides: A process combined by batch experiments and modeling techniques, *J. Mol. Liq.* 215 (2016) 410–416.
- [6] L. Zhang, X. Liu, W. Xia, W. Zhang, Preparation and characterization of chitosan-zirconium(IV) composite for adsorption of vanadium(V), *Int. J. Biol. Macromol.* 64 (2014) 155–161.
- [7] Z. Zhang, H. Zhang, L. Zhu, Q. Zhang, W. Zhu, Hierarchical porous  $\text{Ca}(\text{BO}_2)_2$  microspheres: Hydrothermal–thermal conversion synthesis and their applications in heavy metal ions adsorption and solvent-free oxidation of benzyl alcohol, *Chem. Eng. J.* 283 (2016) 1273–1284.
- [8] H. Al-Zoubi, K.A. Ibrahim, K.A. Abu-Sbeih, Removal of heavy metals from wastewater by economical polymeric collectors using dissolved air flotation process, *J. Water Process Eng.* 8 (2015) 19–27.
- [9] S. Sobhanardakani, H. Parvizmosaed, E. Olyaie, Heavy metals removal from wastewaters using organic solid waste—Rice husk, *Environ. Sci. Pollut. Res.* 20 (2013) 5265–5271.
- [10] T. Madrakian, A. Afkhami, B. Zadbou, M. Ahmadi, New synthetic mercaptoethylamino homopolymer-modified maghemite nanoparticles for effective removal of some heavy metal ions from aqueous solution, *J. Ind. Eng. Chem.* 21 (2015) 1160–1166.
- [11] R. Zandipak, S. Sobhanardakani, Synthesis of  $\text{NiFe}_2\text{O}_4$  nanoparticles for removal of anionic dyes from aqueous solution, *Desalin. Water Treat.* 57 (2016) 11348–11360.
- [12] Y. Ding, L. Zhu, N. Wang, H. Tang, Sulfate radicals induced degradation of tetrabromobisphenol A with nanoscaled magnetic  $\text{CuFe}_2\text{O}_4$  as a heterogeneous catalyst of peroxymonosulfate, *Appl. Catal. B: Environ.* 129 (2013) 153–162.
- [13] W. Pan, F. Gu, K. Qi, Q. Liu, J. Wang, Effect of Zn substitution on morphology and magnetic properties of  $\text{CuFe}_2\text{O}_4$  nanofibers, *Mater. Chem. Phys.* 134 (2012) 1097–1101.
- [14] Z. Huang, G. Yin, X. Liao, Y. Yao, Y. Kang, Preparation and magnetic properties of Cu-ferrite nanorods and nanowires, *J. Colloid Interface Sci.* 317 (2008) 530–535.
- [15] T. Zhang, Q. Li, Y. Liu, Y. Duan, W. Zhang, Equilibrium and kinetics studies of fluoride ions adsorption on  $\text{CeO}_2/\text{Al}_2\text{O}_3$  composites pretreated with non-thermal plasma, *Chem. Eng. J.* 168 (2011) 665–671.
- [16] W. Xu, J. Wang, L. Wang, G. Sheng, J. Liu, H. Yu, X.-J. Huang, Enhanced arsenic removal from water by hierarchically porous  $\text{CeO}_2\text{-ZrO}_2$  nanospheres: Role of surface- and structure-dependent properties, *J. Hazard. Mater.* 260 (2013) 498–507.
- [17] Q. Wang, R. Liu, X. Shen, L. Zou, D. Wu, Mesoporous iron oxide nanofibers and their loading capacity of curcumin, *J. Nanosci. Nanotechnol.* 14 (2014) 2871–2877.
- [18] S. Brunauer, P.H. Emmett, E. Teller, Adsorption of gases in multimolecular layers, *J. Am. Chem. Soc.* 60 (1938) 309–319.
- [19] T. Venkatesha, R. Viswanatha, Y.A. Nayaka, B. Chethana, Kinetics and thermodynamics of reactive and vat dyes adsorption on MgO nanoparticles, *Chem. Eng. J.* 198–199 (2012) 1–10.
- [20] I. Langmuir, The adsorption of gases on plane surfaces of glass, mica and platinum, *J. Am. Chem. Soc.* 40 (1918) 1361–1403.
- [21] H. Freundlich, W. Heller, The adsorption of cis - and trans -azobenzene, *J. Am. Chem. Soc.* 61 (1939) 2228–2230.
- [22] M. Temkin, V. Pyzhev, Recent modifications to Langmuir isotherms, *Acta. Physio. Chim.* 12 (1940) 217–222.
- [23] V.S. Mane, I.D. Mall, V.C. Srivastava, Kinetic and equilibrium isotherm studies for the adsorptive removal of Brilliant Green dye from aqueous solution by rice husk ash, *J. Environ. Manage.* 84 (2007) 390–400.
- [24] S. Azizian, M. Haerifar, J. Basiri-Parsa, Extended geometric method: A simple approach to derive adsorption rate constants of Langmuir–Freundlich kinetics, *Chemosphere* 68 (2007) 2040–2046.
- [25] F. Brouers, O. Sotolongo, F. Marquez, J.-P. Pirard, Microporous and heterogeneous surface adsorption isotherms arising from Levy distributions, *Physica A* 349 (2005) 271–282.
- [26] S. Sobhanardakani, R. Zandipak, 2, 4-Dinitrophenylhydrazine functionalized sodium dodecyl sulfate-coated magnetite nanoparticles for effective removal of Cd (II) and Ni (II) ions from water samples, *Environ. Monit. Assess.* 187 (2015) 1–14.
- [27] T. Sheela, Y.A. Nayaka, R. Viswanatha, S. Basavanna, T. Venkatesha, Kinetics and thermodynamics studies on the adsorption of Zn(II), Cd(II) and Hg(II) from aqueous solution using zinc oxide nanoparticles, *Powder Technol.* 217 (2012) 163–170.
- [28] Y.-Y. Xu, M. Zhou, H.-J. Geng, J.-J. Hao, Q.-Q. Ou, S.-D. Qi, H.-L. Chen, X.-G. Chen, A simplified method for synthesis of  $\text{Fe}_3\text{O}_4@\text{PAA}$  nanoparticles and its application for the removal of basic dyes, *Appl. Surf. Sci.* 258 (2012) 3897–3902.
- [29] S. Sobhanardakani, R. Zandipak, Z. Fili, M. Ghoochian, R. Sahraei, A. Farmany, Removal of V(V) ions from aqueous solutions using oxidized multi-walled carbon nanotubes, *J. Water. Supply. Res T* 64 (2015) 425–433.
- [30] H. Chen, T. Li, L. Zhang, R. Wang, F. Jiang, J. Chen, Pb(II) adsorption on magnetic  $\gamma\text{-Fe}_2\text{O}_3$ /titanate nanotubes composite, *J. Environ. Chem. Eng.* 3 (2015) 2022–2030.
- [31] L. Cui, Y. Wang, L. Gao, L. Hu, L. Yan, Q. Wei, B. Du, EDTA functionalized magnetic graphene oxide for removal of Pb(II), Hg(II) and Cu(II) in water treatment: Adsorption mechanism and separation property, *Chem. Eng. J.* 281 (2015) 1–10.
- [32] S. Zhang, Y. Zhang, J. Liu, Q. Xu, H. Xiao, X. Wang, H. Xu, J. Zhou, Thiol modified  $\text{Fe}_3\text{O}_4@\text{SiO}_2$  as a robust, high effective, and recycling magnetic sorbent for mercury removal, *Chem. Eng. J.* 226 (2013) 30–38.
- [33] Q. Zhao, L. Ren, H. Zhou, T. Cao, P. Chen, Enhanced adsorption of Pb(II) by Al(OH)<sub>3</sub>/(PAA-CO-PAM) sub-microspheres with three-dimensional interpenetrating network structure, *Chem. Eng. J.* 250 (2014) 6–13.
- [34] A. Padilla-Rodríguez, J.A. Hernández-Viezas, J.R. Peralta-Videa, J.L. Gardea-Torresdey, O. Perales-Pérez, F.R. Román-Velázquez, Synthesis of protonated chitosan flakes for the removal of vanadium(III, IV and V) oxyanions from aqueous solutions, *Microchem. J.* 118 (2015) 1–11.
- [35] M.A. Shaker, Adsorption of Co(II), Ni(II) and Cu(II) ions onto chitosan-modified poly(methacrylate) nanoparticles: Dynamics, equilibrium and thermodynamics studies, *J. Taiwan Inst. Chem. Eng.* 57 (2015) 111–122.

- [36] L. Bo, Q. Li, Y. Wang, L. Gao, X. Hu, J. Yang, One-pot hydrothermal synthesis of thrust spherical Mg–Al layered double hydroxides/MnO<sub>2</sub> and adsorption for Pb (II) from aqueous solutions, *J. Environ. Chem. Eng.* 3 (2015) 1468–1475.
- [37] S. Azizian, Kinetic models of sorption: A theoretical analysis, *J. Colloid Interface Sci.* 276 (2004) 47–52.
- [38] A. Marczewski, Application of mixed order rate equations to adsorption of methylene blue on mesoporous carbons, *Appl. Surf. Sci.* 256 (2010) 5145–5152.
- [39] W. Plazinski, W. Rudzinski, A. Plazinska, Theoretical models of sorption kinetics including a surface reaction mechanism: A review, *Adv. Colloid Interface Sci.* 152 (2009) 2–13.
- [40] M. Haerifar, S. Azizian, An exponential kinetic model for adsorption at solid/solution interface, *Chem. Eng. J.* 215–216 (2013) 65–71.
- [41] M. Haerifar, S. Azizian, Fractal-like adsorption kinetics at the solid/solution interface, *J. Phys. Chem. C* 116 (2012) 13111–13119.